

RSC Advances



This is an *Accepted Manuscript*, which has been through the Royal Society of Chemistry peer review process and has been accepted for publication.

Accepted Manuscripts are published online shortly after acceptance, before technical editing, formatting and proof reading. Using this free service, authors can make their results available to the community, in citable form, before we publish the edited article. This *Accepted Manuscript* will be replaced by the edited, formatted and paginated article as soon as this is available.

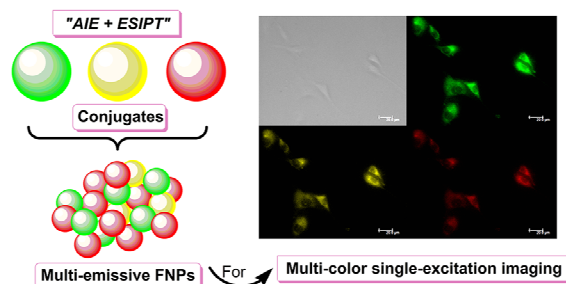
You can find more information about *Accepted Manuscripts* in the [Information for Authors](#).

Please note that technical editing may introduce minor changes to the text and/or graphics, which may alter content. The journal's standard [Terms & Conditions](#) and the [Ethical guidelines](#) still apply. In no event shall the Royal Society of Chemistry be held responsible for any errors or omissions in this *Accepted Manuscript* or any consequences arising from the use of any information it contains.

ENTRY FOR TOC ONLY

Multi-color cell imaging under identical excitation with salicylideneaniline analogues based fluorescent nanoparticles

Hongping Deng, Bing Liu, Chao Yang, Guolin Li,* Yuanyuan Zhuang, Bo Li,* and Xinyuan Zhu*



10 Multi-color cell imaging under identical excitation is realized with fluorescent nanoparticles of salicylideneaniline analogues.

Cite this: DOI: 10.1039/c0xx00000x

www.rsc.org/xxxxxx

ARTICLE TYPE

Multi-color cell imaging under identical excitation with salicylideneaniline analogue based fluorescent nanoparticles

Hongping Deng,^{a1} Bing Liu,^{b1} Chao Yang,^c Guolin Li,^{*b} Yuanyuan Zhuang,^a Bo Li,^{*c} and Xinyuan Zhu^{*a}

Received (in XXX, XXX) Xth XXXXXXXXX 20XX, Accepted Xth XXXXXXXXX 20XX

DOI: 10.1039/b000000x

Six salicylideneaniline (SA) derivatives are synthesized through condensation reaction. Benefiting from their coplanar molecular conformation and intramolecular hydrogen bonds, three compounds are found to exhibit aggregation-induced emission (AIE) or aggregation-induced emission enhancement (AIEE) behavior after self-assembling into nanoparticles with a diameter of about 50 nm. Based on the excited-state intramolecular proton transfer (ESIPT) properties, these fluorescent nanoparticles (FNPs) display green, yellow or orange colors respectively due to the formation of H- or J-aggregates. Interestingly, FNPs derived from BMSpP show green to green-yellow fluorescence because of the partial transform of H-aggregates to J-aggregates. Under neutral condition (pH = 7.4), these FNPs are stable with fluorescence intensity decreasing less than 20% after 120 min compared to the rapid reduction at pH 5.5. Importantly, the two-photon fluorescence property of FNPs originated from salicylideneaniline or its derivatives is firstly reported. The two-photon absorption cross-sections of green, yellow and orange FNPs are tested to be 7, 38 and 27 GM, respectively. After conjugated with phospholipids, these FNPs show good water solubility and low cytotoxicity, which makes them potential candidates for cell imaging application. Finally, multi-color cell imaging under identical excitation with single-emissive and multi-emissive FNPs has been achieved. These results are significant in controlling the one- or two-photon fluorescent properties of these derivatives, and provide a promising platform for multi-color cell imaging application.

Introduction

Over the past years, fluorescent nanoparticles (FNPs) have drawn great attention for their biomedical applications, such as cell-specific targeting,¹ bioanalysis,² detection and identification of proteins³. However, FNPs derived from fluorescent tagging method often suffer some drawbacks.⁴⁻⁵ Self-luminescent quantum dots (QDs) are widely applied for imaging and drug delivery because of their long-term stability and simultaneous detection of multiple signals.⁶ Although QDs are highly fluorescent and photostable, the intrinsic cytotoxicity limits their further bioapplications.^{5, 7} On the other hand, organic dyes are potential candidates for fabricating FNPs due to their excellent optical properties and low toxicity.⁸ Unfortunately, the aggregation of many organic dyes quenches light emission greatly based on the aggregation-caused quenching (ACQ) effect, which prevents the development of emissive nanoparticles.⁹ In 2001, Tang and his coworkers revealed a kind of highly emissive molecule in their aggregated states and defined this phenomenon as aggregation-induced emission (AIE), providing an example to obtain highly emissive FNPs with organic molecules.¹⁰ Since then, multi-color AIE fluorophores were developed and widely used in biosensors and cell imaging applications.¹¹⁻¹² They also further proposed mechanism of AIE effect by a process named restriction of intramolecular rotations (RIR) and revealed that the

E-Z isomerisation was not involved in this process.¹³ However, synthesis of AIE fluorophores with large Stokes shifts in a convenient way is still a great challenge. An efficient method to achieve large Stokes shifts relies on the excited-state intramolecular proton transfer (ESIPT) molecules, which have been reported as near infrared (NIR) or multi-color fluorophores, sensors and white luminescence materials.¹⁴⁻¹⁶

One of the best-known molecules with ESIPT phenomenon is salicylideneaniline (SA), which is the most widely studied photochromic and thermochromic Schiff base.¹⁷⁻¹⁹ Also, many derivatives of SA have been synthesized to study their spectroscopic and photophysical properties. In 2003, Grabowska and coworkers provided the pico- and femtosecond kinetics of the *N,N'*-bis(salicylidene)-*p*-phenylenediamine (BSP), which is a famous symmetric derivative of SA.²⁰ Usually, SA and BSP show very dim fluorescence in solution and few researches focused on their AIE or AIEE properties. In 2004, Yang and coworkers reported the fluorescence enhancement of *N,N'*-bis(salicylidene)-*p*-phenylenediamine (p-BSP) in the nanoparticles compared to that in solution and also proposed a mechanism for the enhanced emission.²¹ Very recently, Ouyang and coworkers controlled the color and morphology of four electron-donor-substituted AIE compounds.²² However, these self-assembled structures are generally very large and lack of water solubility and stability, leading to the impossibility for cell imaging applications. Previously, we developed a macromolecular nanoparticle

approach to obtain FNPs due to RIR of the fluorophore.^{23,24} Therefore, we believe that it will be very convenient to fabricate multi-color FNPs with SA derivatives based on RIR and ESIPT.

In the present work, multi-color FNPs are prepared and applied for multi-color cell imaging using SA derivatives. In details, six SA analogues are easily synthesized through condensation reaction between amino and aldehyde groups. Three of them show bright fluorescence after self-assembled into H- or J-aggregates owing to their coplanar molecular conformation and intramolecular hydrogen bonds. The morphology of these aggregates is spherical with a diameter of about 50 nm, confirmed by transmission electron microscopy (TEM). Moreover, all FNPs have good photostability under neutral condition while pH-responsive properties at acidic environment. Importantly, the two-photon fluorescence of these SA derived FNPs is proved for the first time. To obtain low cytotoxicity and good water solubility, phospholipids are used to encapsulate these FNPs. Finally, multi-color cell imaging under identical excitation is achieved using single-emissive and multi-emissive FNPs.

Experimental section

Materials. p-Phenylenediamine, m-phenylenediamine, o-phenylenediamine, 4-hydroxy benzaldehyde, 3,5-di-tert-butyl-2-hydroxybenzaldehyde, salicylaldehyde and 2-hydroxy-4-methoxybenzaldehyde were purchased from Aladdin and 1,2-dioleoyl-sn-glycero-3-phosphocholine (DOPC) was from Sigma Aldrich. Ethanol (EtOH) was heated at reflux with calcium oxide, and then distilled prior to use. Other reagents and solvents were purchased from Shanghai Sinopharm reagent Co. Ltd., Shanghai, and used without further purification unless otherwise mentioned.

Characterization. Nuclear Magnetic Resonance (NMR). ¹H and ¹³C NMR spectra were tested with a Varian MERCURY plus 400 NMR spectrometer with deuterated chloroform (CDCl₃) or dimethyl sulfoxide-*d*₆ (DMSO-*d*₆) as the solvents at 298 K. The chemical shifts were referenced to residual peaks of deuterated solvents: CDCl₃ (7.26 ppm), DMSO-*d*₆ (2.48 ppm).

Fourier Transform Infrared (FTIR) Spectroscopy. FTIR spectra were performed on a Perkin Elmer Paragon 1000 spectrophotometer between 4000 and 450 cm⁻¹. All sample pellets were prepared by grinding the solid sample with dry potassium bromide (KBr) under high pressure.

High Resolution Mass Spectrometer (HRMS). HRMS was performed on a Waters Micromass Q-TOF Premier Mass Spectrometer. HRMS data were acquired for each sample from 50 to 1000 Da with a 0.10 s scan time and a 0.01 s interscan delay over a 10 min analysis time.

Ultraviolet-Visible (UV-Vis) Absorption Spectra. The UV-Vis absorption spectra of sample solutions were measured at room temperature on a Perkin Elmer Lambda 20 UV-Vis spectrometer in the range of 265-550 nm.

Fluorescence and Quantum Yield Measurements. The fluorescence emission measurements were carried out on a PTI-QM/TM/IM steady-state & time-resolved fluorescence spectrofluorometer (USA/CAN Photon Technology International Int.). Excitation wavelength was $\lambda_{\text{ex}} = 400$ nm. Fluorescence quantum yields were determined using the Rhodamine 6G as the standard ($\lambda_{\text{ex}} = 488$ nm, $\Phi = 0.95$). Quantum yields were

calculated using the same equation and method as depicted in the literature.²⁵

Two-Photon Fluorescence Spectra. The two-photon fluorescence was excited by the fs pulses with different intensities at 800 nm with spectrophotometer (iHR550, HORIBA). The two-photon absorption cross sections were tested with Rhodamine B as the standard.

Transmission Electron Microscopy (TEM). TEM tests were obtained with a JEOL JEM-100CX-II instrument at a voltage of 200 kV. Samples were prepared by drop-casting nano-aggregate solutions onto carbon-coated copper grids and then freeze-drying under vacuum before measurements.

Sample preparations. Preparation of Nano-Aggregates. After all compounds were dissolved in *N,N'*-dimethylformamide (DMF), deionized water was added to the DMF solution via a syringe or washing bottle to form a mixed system. Finally, the mixtures were vibrated with an oscillator or just by hand, respectively. Then, the mixtures were dialyzed with dialysis bag (MWCO = 3,500 Da) for 12 h before measurements if necessary. For pH stability and photostability experiments, the mixture was dialyzed against PBS solution (pH = 7.4) and then added with dilute hydrochloric acid (HCl) to tune the pH to 5.5 when necessary.

Fabrication of Single-Emissive Aggregates. Due to its excellent biocompatibility and water solubility,²⁶ DOPC was chosen to encapsulate different nano-aggregates. Firstly, DOPC was dissolved in methanol/chloroform (v/v = 1:1) mixture and the solvents were removed under reduced pressure to form a thin film. Then, one kind of single nano-aggregate solution was added and kept under ultrasound for 20 min.

Fabrication of Multi-Emissive Aggregates. Briefly, DOPC was dissolved in methanol/chloroform (v/v = 1:1) mixed solvents to form a thin film after removing solvents. Then, three kinds of single aggregate solution were added with a ratio of 3:5:12 (v/v/v) for 4, 5 and 6, respectively. After 20 min sonication, the sample was successfully prepared.

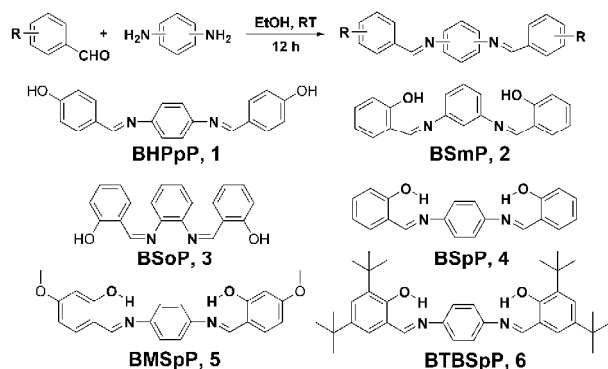
Cell culture and internalization. L929, A549 or MCF-7 cells were seeded in flexiPERM reusable cell culture chambers in combination of glass coverslips and cultured in DMEM (Dulbecco's modified Eagle's medium) (F-12K was used for A549 cells) supplied with 10% FBS (fetal bovine serum) and antibiotics (50 units/mL penicillin and 50 units/mL streptomycin) at 37 °C under a humidified atmosphere containing 5% CO₂. After 24 h of culture, the phospholipid-loaded single- or multi-emissive aggregates were added to culture wells respectively, and the cells were incubated at 37 °C for 15 min or 30 min. Washed with PBS for 3 times, the cells were fixed with 4% formaldehyde for 15 min at room temperature, and then the slides were mounted and observed with a DMI6000B. The excitation wavelength of all samples was 405 nm.

Cytotoxicity measurements of nano-aggregates. The cytotoxicity of single-emissive aggregates was estimated by an MTT viability assay against L929 cells. Firstly, L929 cells were put into 96-well plates with a density of 1×10^4 cells per well in 200 μ L medium. After 24 h, the culture medium was replaced with 200 μ L of a serial aggregate dilutions. The cells were cultured for another 48 h. Then, 20 μ L of 5 mg/mL MTT assays

stock solution in PBS was added to each well. After 4 h, the medium was carefully replaced with 200 μ L of DMSO and the absorbance was tested in a BioTek® Synergy H4 at a wavelength of 490 nm.

5 Results and discussion

SA derivatives were facilely prepared by the synthetic route in Scheme 1. By changing the molecular structures of different reagents, six compounds were synthesized by a conventional condensation of phenylenediamine and phenylaldehyde with good yields (> 95%).²¹⁻²² Details of material synthetic procedures and identifications are shown in the Supporting Information. SA derivatives generally form six-membered-ring intramolecular hydrogen bonds between -OH groups and the N atoms, which can be confirmed by ¹H NMR spectra (Fig. 1A).¹⁴ Compound BHPpP (1) exhibits a phenol signal only at 10.10 ppm for the incapacity of forming intramolecular hydrogen bonds. Compared to BHPpP, other compounds show significant downfield phenol signals from 12.93 ppm to 13.93 ppm, giving an obvious indication of the formation of strong hydrogen bonds. It is clear that stronger electron donating abilities result in lower downfield phenol signals. Their structure was further characterized by FTIR and ¹³C NMR (Fig. 1B and Fig. S1).



Scheme 1 The synthetic route and chemical structures of SA derivatives BHPpP (1), BSmp (2), BSoP (3), BSpP (4), BMSpP (5) and BTBSpP (6).

To explore the potential optical properties of six compounds, UV absorbance spectra were tested and shown in Fig. 2A. Compound BHPpP has two absorption bands at about 293 nm and 361 nm, respectively, ascribing to the electron transition of π - π^* and n - π^* . Compared to BHPpP, the n - π^* transition absorption of BSpP (4) red-shifts to 371 nm while that of the π - π^* blue-shifts to 276 nm, which can be attributed to the interactions of six-membered-ring intramolecular hydrogen bonds. However, the n - π^* transition absorption of compounds BSmp (2) and BSoP (3) still presents blue-shift phenomenon with the formation of intramolecular hydrogen bonds, which is ascribed to the destruction of coplanar conformation of the molecules. As a matter of course, the increased electron donating abilities of BMSpP (5) and BTBSpP (6) result in the red-shifts of both π - π^* and n - π^* absorptions. Surprisingly, the DMF solution of all compounds shows very weak or even undetectable fluorescence at room temperature. Considering that SA compounds demonstrate AIE or AIEE characteristics,²¹⁻²² we believe that these SA analogues also have great potential as AIE or AIEE

fluorophores by RIR.

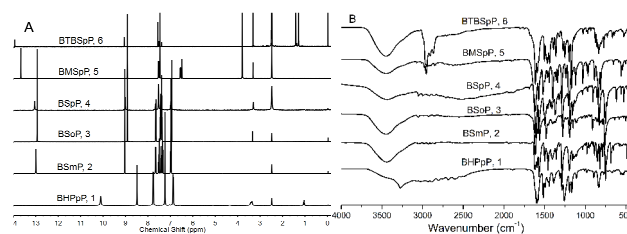


Fig. 1 ¹H NMR and FTIR spectra of salicylideneaniline derivatives BHPpP (1), BSmp (2), BSoP (3), BSpP (4), BMSpP (5) and BTBSpP (6).

The AIE or AIEE characteristics of compounds 1-3 were investigated in DMF/H₂O solutions. Figure 2B presents the UV absorbance spectra of BHPpP in different DMF/H₂O mixtures. BHPpP has two absorption peaks as mentioned above in pure DMF. However, the second absorption peak which belongs to n - π^* transition gradually disappears with the increase of water contents, strongly indicating the breakage of C=N bonds. Indeed, the UV absorption spectrum of BHPpP in DMF/H₂O (1/99) is the same as that of reaction starting materials. The lack of six-membered-ring intramolecular hydrogen bonds leads to the fast breakage of C=N bonds for BHPpP. For compounds BSmp and BSoP, the destruction of coplanar conformation results in the heterogeneous formation of J- or H-aggregates, which can be confirmed by the UV absorbance spectra with both red- and blue-shift characteristics (Fig. 2C and Fig. 2D).²⁷⁻²⁹ Thus, the nano-aggregates of both BSmp and BSoP show undetectable fluorescence in all DMF/H₂O solution. In principle, compounds 1-3 act as references to emphasize the importance of intramolecular hydrogen bonds and coplanar molecular conformation on the AIE or AIEE properties.

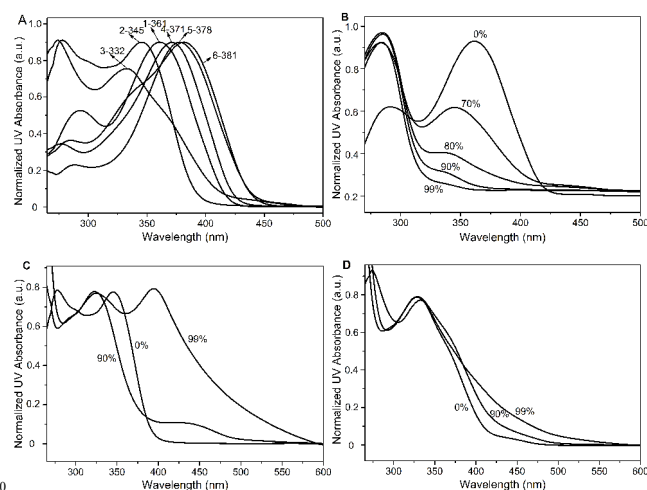


Fig. 2 UV spectra of salicylideneaniline derivatives: (A) BHPpP (1), BSmp (2), BSoP (3), BSpP (4), BMSpP(5) and BTBSpP (6) in DMF; (B) BHPpP (1) in DMF/H₂O mixture; (C) BSmp (2) in DMF/H₂O mixture; (D) BSoP (3) in DMF/H₂O mixture. Water contents (%) are listed.

Furthermore, the AIE or AIEE characteristics of compounds 4-6 were investigated in details. In fact, BSpP was an accidental discovery which shows an obvious AIE yellow fluorescence after self-assembling into nano-aggregates. Under lower water content (< 75%), the UV peak displays both blue- and red-shift potential

compared to that in DMF, which can be regarded as a non-equilibrium state. However, clear red-shifted UV peak (about 70 nm) in higher water content indicates the formation of J-aggregates which is more perfect under 90% water content with a relatively better buffer capacity compared to 99% one (Fig. 3A).

Moreover, BSpP has undetectable fluorescence in DMF at room temperature. When water (a poor solvent for BSpP) is added to the DMF solution, the emission intensity grows drastically with higher water content, giving a transparent AIE active feature (Fig. 3B).¹⁰⁻¹² The emission peak is at 547 nm, giving a large Stokes shift (147 nm) owing to the ESIPT effect.^{14,16} With 99% water content, the emission intensity decreases due to the formation of less ordered J-aggregates. Based on these results, BMSpP and BTBSpP were further designed and prepared by using different salicylaldehyde substituents and their optical properties were also investigated. Compared to BSpP in mixed DMF/H₂O solvents, the UV absorption peak of BMSpP blue-shifts about 55 nm with the increase of water content (Fig. 3C), which gives clear confirmation of the formation of H-aggregates.²⁹ Moreover, the DMF solution of BMSpP shows weak green fluorescence with an emission peak at about 511 nm. With the growth of water content to 90%, the fluorescence intensity increases greatly and the emission peak displays a 6 nm red-shift; while with 99% water content, the fluorescence intensity decreases drastically and the emission peak has further 4 nm red-shift (Fig. 3D). The above experiment results indicate that BMSpP works with an AIEE character and higher (99%) water content was not preferable for the formation of ordered H-aggregates. It is amazing that the nano-aggregates of BMSpP show green-yellow fluorescence with an emission peak at about 525 nm using a much faster water adding speed (Fig. S2). However, the green-yellow fluorescence rapidly vanishes within hours, indicating the formation of unstable aggregates. The UV absorption spectra of BTBSpP in DMF and lower water content (below 80%) are almost identical and only show about 10 nm red-shifts with high water content (above 90%), demonstrating the formation of weak J-aggregates due to the steric hindrance of tert-butyl groups (Fig. 3E). The fluorescence emission spectra of BTBSpP in DMF show clear emission peak at about 574 nm and the emission intensity increases with higher water content, which confirms the AIEE feature.¹⁰⁻¹² Just as BSpP and BMSpP, the emission intensity decreases with higher water content for BTBSpP, but without obvious emission peak shifts (Fig. 3F). To illustrate the generalization of AIE or AIEE properties of compounds 4-6, the fluorescence enhancement features for the corresponding FNPs in THF/H₂O and DMSO/H₂O mixtures were also measured and shown in Figure S4. From the results, it is clear that the fluorescence enhancement behavior is obvious in all mixed solvents. Thus, the highest fluorescence quantum yields (QYs) of green, yellow and orange FNPs were tested to be 0.10, 0.26 and 0.02, respectively (Table S1). Subsequently, transmission electron microscopy (TEM) measurements were applied to illustrate the morphology of FNPs with highest QYs (Fig. S3). All of the aggregates present spherical structure with a diameter of about 57 nm, 52 nm, and 48 nm for BSpP, BMSpP and BTBSpP, respectively. To make it more intuitionistic, the UV-Vis, fluorescence and two-photon properties along with size of all three FNPs are listed and presented in Table S1.

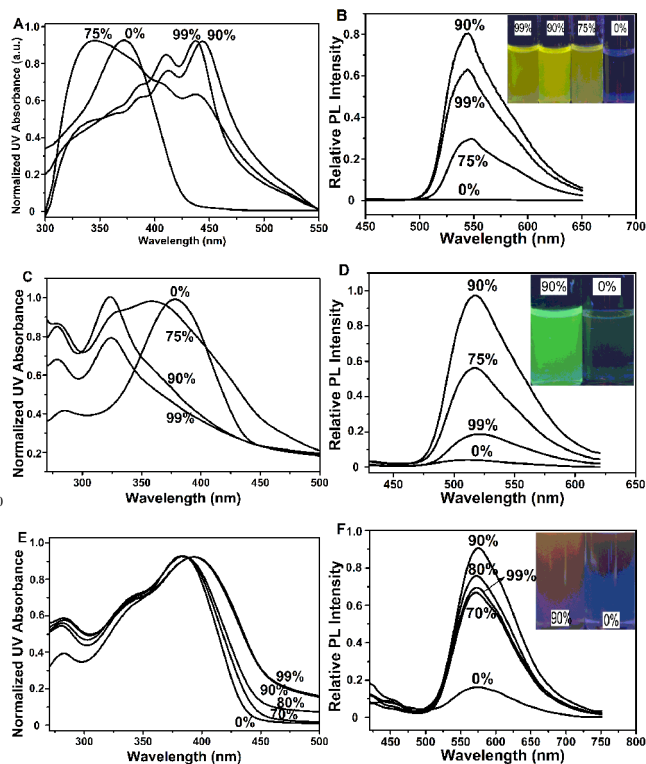


Fig. 3 Normalized UV absorbance and fluorescence emission spectra of SA derivatives BSpP (4), BMSpP (5) and BTBSpP (6) in DMF/H₂O mixtures (10 μ M, λ_{ex} = 400 nm) with varied volumetric fractions of water: BSpP (A and B), BMSpP (C and D), and BTBSpP (E and F).

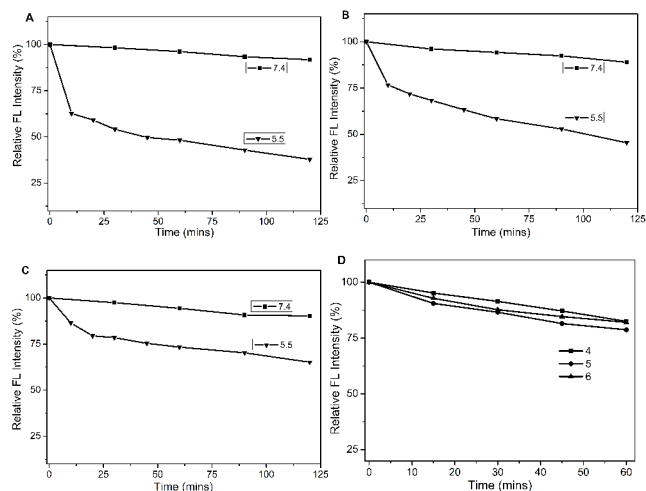


Fig. 4 Fluorescence stability studies under neutral (pH = 7.4) and acidic (pH = 5.5) conditions: BSpP, 4 (A), BMSpP, 5 (B) and BTBSpP, 6 (C), and photostability of nano-aggregates (D, pH = 7.4).

To confirm the formation of H- or J-aggregates of these compounds, concentration-dependent UV-Vis absorption and steady state fluorescence spectra were tested in different mixed solvents. Figure S5 gives the corresponding results in DMF/H₂O mixed solvents. At low concentration, the absorption peak of BSpP nanoparticles is at about 362 nm. With the increase of concentration, obvious red-shift of absorption peak is clearly seen with a Stokes shift of about 68 nm, confirming the formation of J-aggregates. However, the fluorescence can not be seen under low

concentration. For BMSpP nanoparticles, clear blue-shift of the absorption peak with increasing concentration affirms the formation of H-aggregates. In accord with absorption, the fluorescence peak also show about 3 nm blue-shift with higher concentration, confirming the formation of H-aggregates. Moreover, the absorption and fluorescence peaks of BTBSpP nanoparticles also display weak bathochromic-shift along with increasing concentration, which indicates the formation of weak J-aggregates. Finally, concentration-dependent absorption and fluorescence spectra were further detected in DMSO/H₂O and THF/H₂O mixed solvents (Fig. S6 and Fig. S7), and almost the same phenomena were observed for these systems, which further illustrated the formation of H- or J-aggregates for these compounds.

Considering that SA analogues were connected by imine bonds, the pH-responsive properties of nano-aggregates with different colors were studied in PBS solutions. As shown in Figure 4, all of three nano-aggregates are very stable at pH = 7.4 with fluorescence intensity decrease less than 20% after 120 min compared to the rapid degradation of BHPpP (1). However, the fluorescence intensity fades rapidly under acidic conditions at pH = 5.5, especially during the first 25 min. Moreover, the fading speed of fluorescence intensity decreases from BSpP to BTBSpP, indicating the steric hindrance effect for substituent groups toward the migration of protons. Afterwards, the photostability of three nano-aggregates in PBS solution at pH = 7.4 was explored and shown in Fig. 4D. In general, three nano-aggregates show good photostability with more than 80% fluorescence intensity left after 60 min irradiation with 365 nm lamp.

To our surprising, all of three SA derived FNPs exhibit two-photon fluorescence properties, which have never been reported for SA and its derivatives. As shown in Figure 5, the two-photon emission spectra are recorded under different radiation power. With the increase of radiation power, the emission intensity increases. The good linear correlation between intensity (area) and square of pump power affirms the two-photon emission properties of three FNPs. In addition, the two-photon absorption cross-sections are tested to be 38, 7 and 27 GM for BSpP, BMSpP, and BTBSpP nanoparticles, respectively.

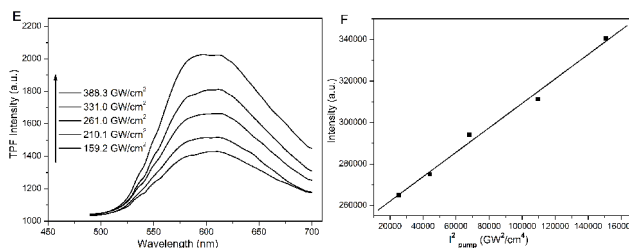
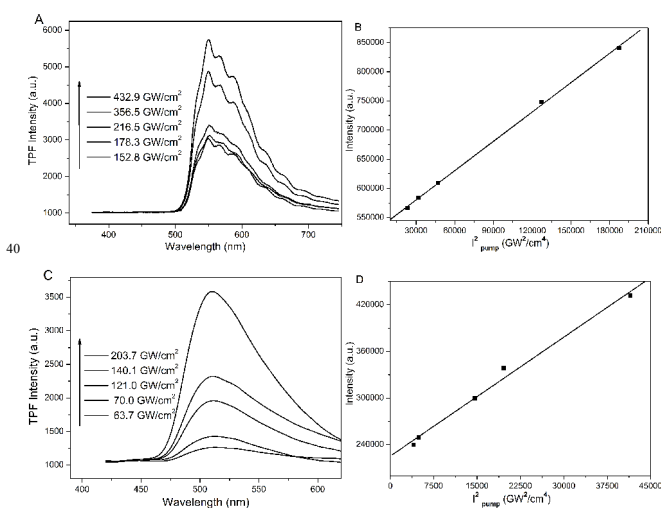


Fig. 5 Two-photon fluorescence emission (A, C, E) and the corresponding linear fitting (B, D, F) spectra of BSpP, BMSpP, and BTBSpP under different excitation power: BSpP (A and B), BMSpP (C and D), and BTBSpP (E and F).

Benefiting from their bright and multi-color fluorescence, we tend to use three kinds of SA FNPs for cell imaging. However, all of three FNPs were unstable and aggregated in the cell culture medium, which inhibited their cell applications. To solve this problem, commercial phospholipids were employed to regulate the cell entrance of nanoparticles due to their good biocompatibility and water solubility.²⁶ As shown in Figure S8, the phospholipid-encapsulated FNPs present little cytotoxicity towards L929 cells even with the highest concentration (10 μ M). Subsequently, A549 and MCF-7 cells were cultured with single-emissive nanoparticles and bright fluorescence could be observed after 15 min or 30 min (Figure S9). The fluorescence is almost in the cytoplasm of both cells. Moreover, multi-emissive nanoparticles were prepared by mixing the green, yellow and orange FNPs and then encapsulated with phospholipids. Thus, the multi-emissive nanoparticles were applied in multi-color cell imaging under the same excitation. As depicted in Figure 6, green, yellow and red fluorescence is very obvious for A549 and MCF-7 cells after 15 min and 30 min culture. Indeed, the fluorescence signals are from the multi-emissive nanoparticles with the same excitation wavelength, which can raise the analysis reliability and facticity.³⁰

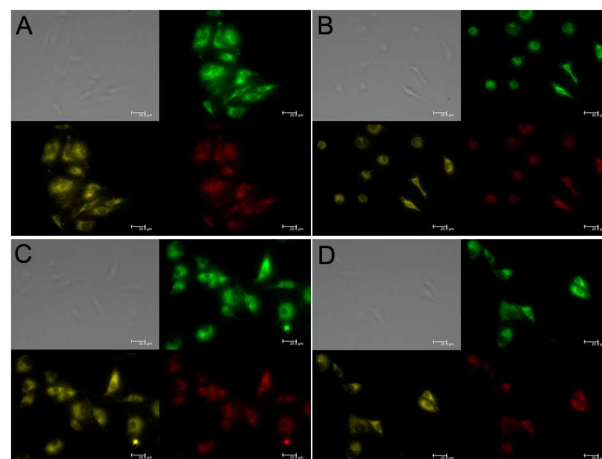


Fig. 6 Multi-color fluorescence imaging of A549 (A and B) and MCF-7 (C and D) cells using multi-emissive FNPs for 15 min (A and C) and 30 min (B and D) with green, yellow and red channels under identical excitation. Scale bar = 20 μ m. Concentration = 2 μ M, λ_{ex} = 405 nm.

Conclusions

In conclusion, six SA derivatives are easily synthesized by traditional condensation reactions with high yields. Due to the

ESIPT phenomenon, three chromophores with more coplanar structure show AIE or AIEE feature after self-assembling into H- or J-aggregates. Moreover, the two-photon fluorescence of three SA aggregates is confirmed for the first time. Finally, multi-color fluorescence imaging with multi-emissive nano-aggregates is successfully achieved under identical excitation using A549 and MCF-7 cells.

Acknowledgement

This work was financially supported by the National Basic Research Program (2015CB931801, 2012CB821500, 2013CB834506), and National Natural Science Foundation of China (51473093).

Notes and references

^aSchool of Chemistry and Chemical Engineering, State Key Laboratory of Metal Matrix Composites, Shanghai Jiao Tong University, 800 Dongchuan Road, Shanghai 200240, P. R. China. Fax: +86-21-54741297; Tel: +86-21-34203400; E-mail: xyzhu@sjtu.edu.cn

^bDepartment of Oral and Maxillofacial Surgery, The First Affiliated Hospital of Harbin Medical University, 23 Youzheng Street, Nangang District, Harbin 150001, P. R. China. Fax: +86-21-54741297; Tel: +86-21-34203400; E-mail: liguolin@126.com

^cKey Laboratory of Polar Materials and Devices, Ministry of Education, East China Normal University, Shanghai 200241, P. R. China. Fax: +86-21-54741297; Tel: +86-21-34203400; E-mail: bli@ee.ecnu.edu.cn

^dThese authors contributed equally to this work.

† Electronic Supplementary Information (ESI) available: ¹³C NMR spectra, TEM data, MTT assay and other characterizations. This material is available free of charge via the Internet. See DOI: 10.1039/b000000x/

- 1 R. Weissleder, K. Kelly, E. Y. Sun, T. Shtatland and L. Josephson, *Nat. Biotechnol.*, 2005, **23**, 1418.
- 2 R. Gill, M. Zayats and I. Willner, *Angew. Chem. Int. Ed.*, 2008, **47**, 7602.
- 3 C. -C. You, O. R. Miranda, B. Gider, P. S. Ghosh, I. -B. Kim, B. Erdogan, S. A. Krovi, U. H. F. Bunz and V. M. Rotello, *Nat. Nanotechnol.*, 2007, **2**, 318.
- 4 C. R. Jing and V. W. Cornish, *Acc. Chem. Res.*, 2011, **44**, 784.
- 5 X. D. Xue, Y. Y. Zhao, L. L. Dai, X. Zhang, X. H. Hao, C. Q. Zhang, S. D. Huo, J. Liu, C. Liu, A. Kumar, W. -Q. Chen, G. Z. Zou and X. -J. Liang, *Adv. Mater.*, 2014, **26**, 712.
- 6 I. L. Medints, H. T. Uyeda, E. R. Goldman and H. Mattoussi, *Nat. Mater.*, 2005, **4**, 435.
- 7 K. T. Yong, W. C. Law, R. Hu, L. Ye, L. W. Liu, M. T. Swihart and P. N. Prasad, *Chem. Soc. Rev.*, 2013, **42**, 1236.
- 8 L. Yuan, W. Y. Lin, K. B. Zheng, L. W. He and W. M. Huang, *Chem. Soc. Rev.*, 2013, **42**, 622.
- 9 W. Z. Yuan, P. Lu, S. Chen, J. W. Y. Lam, Z. Wang, Y. Liu, H. S. Kwok, Y. Ma and B. Z. Tang, *Adv. Mater.*, 2010, **22**, 2159.
- 10 J. Luo, Z. Xie, J. W. Y. Lam, L. Cheng, H. Chen, C. Qiu, H. S. Kwok, X. Zhan, Y. Liu, D. Zhu and B. Z. Tang, *Chem. Commun.*, 2001, 1740.
- 11 Y. Liu, C. M. Deng, L. Tang, A. J. Qin, R. R. Hu, J. Z. Sun and B. Z. Tang, *J. Am. Chem. Soc.*, 2011, **133**, 660.
- 12 C. W. T. Leung, Y. N. Hong, S. J. Chen, E. G. Zhao, J. W. Y. Lam and B. T. Tang, *J. Am. Chem. Soc.*, 2013, **135**, 62.
- 13 N. W. Tseng, J. Z. Liu, J. C. Y. Ng, J. W. Y. Lam, H. H. Y. Sung, I. D. Williams and B. Z. Tang, *Chem. Sci.*, 2012, **3**, 493.
- 14 K. C. Tang, M. J. Chang, T. Y. Lin, H. A. Pan, T. C. Fang, K. Y. Chen, W. Y. Huang, Y. H. Hsu and P. T. Chou, *J. Am. Chem. Soc.*, 2011, **133**, 17738.
- 15 D. Maity, V. Kumar and T. Govindaraju, *Org. Lett.*, 2012, **14**, 6008.
- 16 S. Park, J. E. Kwon and S. Y. Park, *Phys. Chem. Chem. Phys.*, 2012, **14**, 8878.

- 17 E. Hadjoudis and I. M. Mavridis, *Chem. Soc. Rev.*, 2004, **33**, 579.
- 18 M. Z. Zgierski and A. Grabowska, *J. Chem. Phys.*, 2000, **112**, 6329.
- 19 V. Vargas, *J. Phys. Chem. A*, 2004, **108**, 281.
- 20 M. Zótek, J. Kubicki, A. Maciejewski, R. Naskręcki and A. Grabowska, *Chem. Phys. Lett.*, 2003, **369**, 80.
- 21 S. Y. Li, L. M. He, F. Xiong, Y. Li and G. Q. Yang, *J. Phys. Chem. B*, 2004, **108**, 10887.
- 22 C. X. Niu, L. Zhao, T. Fang, X. B. Deng, H. Ma, J. X. Zhang, N. Na, J. S. Han and J. Ouyang, *Langmuir* 2014, **30**, 2351.
- 23 H. P. Deng, Q. Zhu, D. L. Wang, C. L. Tu, B. S. Zhu and X. Y. Zhu, *Polym. Chem.*, 2012, **3**, 1975.
- 24 Y. J. Zheng, G. L. Li, H. P. Deng, Y. Su, J. H. Liu and X. Y. Zhu, *Polym. Chem.*, 2014, **5**, 2521.
- 25 A. Baldrige, S. H. Feng, Y. -T. Chang and L. M. Tolbert, *ACS Comb. Sci.*, 2011, **13**, 214.
- 26 K. Raemdonck, K. Braechmans, J. Demeester and S. C. D. Smedt, *Chem. Soc. Rev.*, 2014, **43**, 444.
- 27 T. E. Kaiser, V. Stepanenko, F. Würthner, *J. Am. Chem. Soc.*, 2009, **131**, 6719.
- 28 F. Würthner, T. E. Kaiser and C. R. Saha-Möller, *Angew. Chem. Int. Ed.*, 2011, **50**, 3376.
- 29 R. J. Dong, B. S. Zhu, Y. F. Zhou, D. Y. Yan and X. Y. Zhu, *Angew. Chem. Int. Ed.*, 2012, **51**, 11633.
- 30 F. C. Alexandra, M. S. Chad, N. Iulija, P. Stéphane and V. E. Svetlana, *Angew. Chem. Int. Ed.*, 2014, **53**, 2927.